Surface & Coatings Technology 259 (2014) 495–499

Contents lists available at ScienceDirect

Surface & Coatings Technology

journal homepage: www.elsevier.com/locate/surfcoat

Energetically deposited nano-composite films of high speed steel and titanium nitride

A.M. Pagon, D.G. McCulloch *, E.D. Doyle, J.G. Partridge

School of Applied Sciences, RMIT University, GPO Box 2476, Melbourne, 3001 Victoria, Australia

ARTICLE INFO

Article history:
Received 26 June 2014
Accepted in revised form 17 October 2014
Available online 23 October 2014

Keywords:
Nano-composites
Filtered cathodic vacuum arc
Microstructure
Nanoindentation
Electron microscopy

ABSTRACT

A filtered cathodic vacuum arc system has been used to reactively deposit nano-composite high speed steel (HSS)-TiN films from a cold-sprayed HSS-Ti cathode. The microstructure of the films depended on both the energy of the depositing flux (controlled by substrate bias) and the substrate temperature. With a low substrate bias of −25 V at room temperature, a fine nanocrystalline microstructure was produced. An increase in preferred orientation of the FCC TiN phase was observed in films deposited at RT with elevated substrate biases. Elevated temperature in the absence of bias promoted orientation of the BCC Fe phase. Moderate substrate bias (~−200 V) and high substrate temperature (>250 °C) improved the hardness, elastic modulus and elastic recovery of the HSS-TiN thin films. Potential applications for these films, with tunable mechanical properties, include matching layers between HSS tools and TiN protective coatings.

1. Introduction

Nano-composite tribological coatings, deposited by physical vapour deposition (PVD) or chemical vapour deposition, have exhibited impressive physical and chemical properties including extremely high indentation hardness (40–80 GPa) [1–3], corrosion resistance [4,5], excellent high temperature oxidization resistance [6,7] and high abrasion/erosion resistance [8–10]. Compositionally and/or structurally graded nano-composite coatings have the potential to improve property matching at coating/substrate interfaces. For example, in a nano-composite coating consisting of a mixture of a nitride forming metal and a non-nitride forming metal, if the non-nitride forming metallic element is of the same composition as the substrate and/or falls within the Hume–Rothery rules for solid solubility [11], a graded interface can be formed. This approach has been used by Jewsbury et al. [12], who reported the formation of graded interfaces between a substrate and a hard compound coating ablated from a composite Ti/Ni cathode using a steered cathodic arc. This work suggests that similar methods could be employed to reduce the steep property gradients existing at other substrate/PVD interfaces.

In this study, we have investigated PVD HSS-TiN nano-composite coatings with a view to improving the performance of high speed steel (HSS) cutting tools. Nano-composite HSS-Ti and HSS-TiN films were deposited energetically within a filtered cathodic vacuum arc (FCVA) system equipped with a single HSS/Ti cathode. In a FCVA system, the average energy of the depositing flux can be controlled using a substrate bias, enabling a greater variety of microstructures to be synthesized at moderate temperatures [13]. Consequently, FCVA deposition is well suited to the investigation of nano-composite films. Multi-element cathodes are typically fabricated by hot-pressing powders of multiple elements under high-temperature and high-pressure conditions. Here, the HSS-Ti cathode was fabricated using the cold gas-dynamic spray or 'cold-spray' technique [11,14], used previously to produce sputtering targets [15] and cathodes within an atmospheric pressure arc system [16]. This approach enabled deposition of HSS-Ti from a largely non-magnetic cathode, critical for stable operation of a cathodic arc.

2. Material and methods

Films were prepared using an FCVA deposition system [17], operating with an arc current of 100 A. A magnetic double bend filter connecting the source and deposition chambers minimized the deposition of macroparticles. Polished silicon wafer substrates were cleaned with acetone and ethanol and mounted on a bias-compatible, resistive filament, substrate heater/holder within the FCVA system prior to deposition. The FCVA was then pumped to a base pressure of less than 10^{-3} Pa. The nano-composite films of HSS/TiN were all deposited from the HSS/Ti cathode in a 0.29 Pa N_2 and 0.013 Pa Ar atmosphere (Ar/N_2 flow rates 5/60 sccm). For comparison purposes, a TiN film was deposited using a Ti cathode under similar conditions and a HSS/Ti film was deposited in an inert 0.30 Pa Ar atmosphere. The ion beam current density at the substrate (measured using an electrometer built into the bias power supply) was less than 1.0 mA/cm^2 during all depositions. A schematic of the HSS/Ti cathode is shown in Fig. 1(a). Concentric channels of depth 5 mm were cut into a Ti solid cathode and subsequently filled with cold-sprayed HSS, resulting in the cathode

* Corresponding author. Tel.: +61 3 99253391; fax: +61 3 9925 5290.
E-mail address: dougal.mcculloch@rmit.edu.au (D.G. McCulloch).

http://dx.doi.org/10.1016/j.surfcoat.2014.10.041
0257-8972/

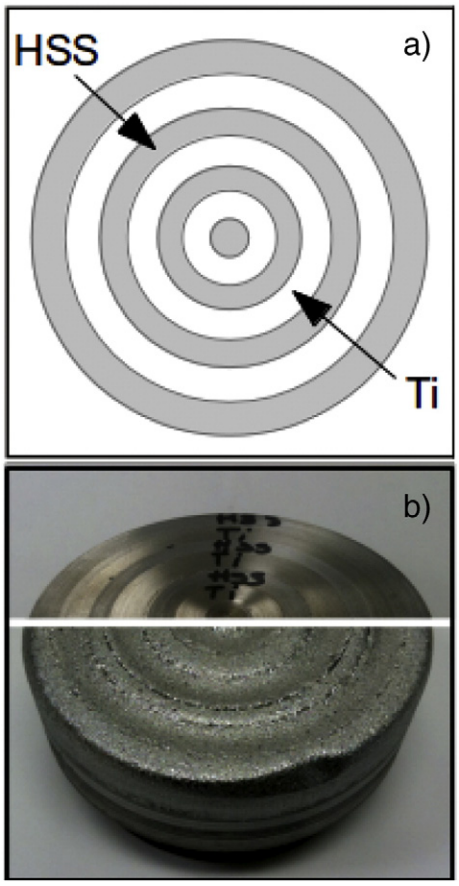

Fig. 1. (a) Plan view schematic and (b) photograph of the HSS/Ti cathode before (upper) and after deposition of films (lower).

shown in the upper part of the photograph shown in Fig. 1(b). The surface areas of the HSS and Ti sections were approximately equal. A series of films was prepared using different substrate bias and heater temperatures, as shown in Table 1. The surface temperature of the substrate measured during deposition using a thermocouple mounted on a separate silicon substrate was less than 35 °C during all depositions. The cathode exhibited uniform erosion during our depositions. After all depositions were complete, some preferential erosion of the HSS was observed at the edges of the tracks as shown in the lower part of Fig. 1(b).

Using Stoney's equation [18] and a Tencor surface profiler, the intrinsic stress in each film was determined from the radii of curvature of the substrates (measured before and after deposition) and the film thickness. Surface roughness was measured using a Veeco Dimension 3100 atomic force microscope (AFM) operated in tapping mode and calculated from 10 × 10 μm square areas. The depth dependent compositions of the thin films were determined using a Thermo Scientific K-Alpha X-ray photo-electron Spectrometer (XPS) equipped with an Al anode X-ray source and with an Ar ion beam operating at 1–2 keV. The C1s peak (284.8 eV) was used as a reference for the XPS peak positions.

X-ray diffraction (XRD) data was collected using a Bruker D8 DISCOVER microdiffractometer fitted with a GADDS (General Area Detector Diffraction System), using CuKα radiation. Cross-section TEM specimens were prepared using a combination of mechanical polishing and Ar ion beam etching. The specimens were imaged using a JEOL2010 TEM operating at 200 kV.

The mechanical properties of the thin films were studied using a Hysitron 950 Triboindenter fitted with a Berkovich indentation tip. To determine the hardness, H and effective elastic modulus, E*, twenty-five indents were made up to a maximum force of 1000 μN and hardness values were calculated using the Oliver and Pharr method [19]. The maximum penetration depth was ~55 nm. The elastic recoveries (w_p) of the coatings were calculated from load–unload curves [20].

3. Results & discussion

Table 1 includes the deposition rates and average thickness of all films. The HSS/TiN deposition rate decreased with increasing bias, attributable to increased sputtering due to the increased ion energy at higher bias. The decrease in deposition rate with increased temperature suggests re-evaporation from the growing film, often observed in PVD. Table 1 includes the RMS roughness of all films. The thin films deposited at lower substrate bias (<−300 V) exhibited smooth surfaces with roughness less than 0.2% of the film thickness. The films deposited at biases >−300 V exhibited higher surface roughness as did the film deposited at −25 V bias, 500 °C. In summary, the film roughness increases with bias and/or temperature. These dependencies have been observed before. Tay et al. [21] found that in TiN, grain size increased with bias, as did surface roughness. In energetically deposited TiN–Ni nanocomposite thin films, the roughness increased with temperature [22].

Fig. 2 shows the composition versus depth of selected films, obtained using XPS depth profiling. All films exhibited very high oxygen levels (~70%) at their surfaces, consistent with the presence of a thin surface oxide layer. This was expected, as the constituent materials oxidise readily. The composition calculated from this surface scan was omitted from Fig. 2 for clarity. The average compositions of the main constituents of the films are summarised in Table 2. The compositions of both the HSS-Ti and HSS-TiN films were found to be Fe rich when compared to the surface areas of Fe and Ti in the cathode which were approximately equal. This difference is attributed to the higher cohesive energy of Ti leading to preferential ablation of HSS (4.85 eV compared with 4.28 eV) [23]. Importantly, the composition of the films remains approximately constant as the cathode is eroded throughout the sequence of depositions. The nitrogen rich processing environment used to deposit the HSS-TiN films does not greatly alter the Fe/Ti ratio. The concentration of nitrogen in these films was found to be approximately equal to

Table 1
Deposition, structural and mechanical properties of films produced from the HSS-Ti cold-sprayed cathode including surface roughness, stress, hardness (H), effective elastic modulus (E*) and elastic recovery (w_p). RT = room temperature.

Film type	Bias (V)	Temp. (°C)	Thick. (nm)	Dep. rate (nm/min)	Surface rough. (nm)	Stress (GPa)	H (GPa)	E* (GPa)	w_p
HSS-Ti	−25	RT	265	88	0.5	0.6	11.7	160	0.53
HSS-TiN	−25	RT	160	64	0.3	1.3	13.6	195	0.56
HSS-TiN	−100	RT	200	50	0.3	2.3	15.7	205	0.60
HSS-TiN	−200	RT	285	48	0.5	2.1	17.1	205	0.61
HSS-TiN	−300	RT	255	38	0.9	1.5	17.3	200	0.61
HSS-TiN	−400	RT	265	38	0.9	1.4	17.5	205	0.66
HSS-TiN	−500	RT	105	35	0.7	2.1	18.6	205	0.69
HSS-TiN	−25	250	260	52	0.3	1.3	13.2	200	0.50
HSS-TiN	−25	500	200	40	0.8	−0.4	19.5	224	0.67
TiN	−25	RT	270	50	0.9	6.4	30.0	271	0.71